

Ferhun C. Caner¹

Ramón y Cajal Researcher and Lecturer
School of Civil Engineering,
Technical University of Catalonia (UPC),
Jordi Girona 1-3,
Barcelona, Spain 08034;
Formerly Visiting Scholar,
Department of Civil and Environmental
Engineering,
Northwestern University,
2145 Sheridan Road, Evanston, Illinois 60208
e-mail: ferhun.caner@upc.edu

Zaoyang Guo

Lecturer
Department of Mechanical and Civil Engineering,
University of Glasgow,
G12 8LT Glasgow, Scotland;
Formerly Research Associate,
Department of Mechanical Engineering,
Northwestern University,
2145 Sheridan Road,
Evanston, Illinois 60208
e-mail: z.guo@eng.gla.ac.uk

Brian Moran

Professor
e-mail: b-moran@northwestern.edu

Zdeněk P. Bažant

Walter P. Murphy Professor of Civil Engineering
and Materials Science
e-mail: z-bazant@northwestern.edu

Department of Civil and Environmental
Engineering,
Northwestern University,
2145 Sheridan Road,
Evanston, Illinois 60208

Ignacio Carol

Professor
School of Civil Engineering,
Technical University of Catalonia (UPC),
Jordi Girona 1-3,
Barcelona, Spain 08034
e-mail: ignacio.carol@upc.edu

Hyperelastic Anisotropic Microplane Constitutive Model for Annulus Fibrosus

In a recent paper, Peng et al. (2006, "An Anisotropic Hyperelastic Constitutive Model With Fiber-Matrix Interaction for the Human Annulus Fibrosus," ASME J. Appl. Mech., 73(5), pp. 815–824) developed an anisotropic hyperelastic constitutive model for the human annulus fibrosus in which fiber-matrix interaction plays a crucial role in simulating experimental observations reported in the literature. Later, Guo et al. (2006, "A Composites-Based Hyperelastic Constitutive Model for Soft Tissue With Application to the Human Fibrosis," J. Mech. Phys. Solids, 54(9), pp. 1952–1971) used fiber reinforced continuum mechanics theory to formulate a model in which the fiber-matrix interaction was simulated using only composite effect. It was shown in these studies that the classical anisotropic hyperelastic constitutive models for soft tissue, which do not account for this shear interaction, cannot accurately simulate the test data on human annulus fibrosus. In this study, we show that the microplane model for soft tissue developed by Caner and Carol (2006, "Microplane Constitutive Model and Computational Framework for Blood Vessel Tissue," ASME J. Biomech. Eng., 128(3), pp. 419–427) can be adjusted for human annulus fibrosus and the resulting model can accurately simulate the experimental observations without explicit fiber-matrix interaction because, in microplane model, the shear interaction between the individual fibers distributed in the tissue provides the required additional rigidity to explain these experimental facts. The intensity of the shear interaction between the fibers can be adjusted by adjusting the spread in the distribution while keeping the total amount of the fiber constant. A comparison of results obtained from (i) a fiber-matrix parallel coupling model, which does not account for the fiber-matrix interaction, (ii) the same model but enriched with fiber-matrix interaction, and (iii) microplane model for soft tissue adapted to annulus fibrosus with two families of fiber distributions is presented. The conclusions are (i) that varying degrees of fiber-fiber and fiber-matrix shear interaction must be taking place in the human annulus fibrosus, (ii) that this shear interaction is essential to be able to explain the mechanical behavior of human annulus fibrosus, and (iii) that microplane model can be fortified with fiber-matrix interaction in a straightforward manner provided that there are new experimental data on distribution of fibers, which indicate a spread so small that it requires an explicit fiber-matrix interaction to be able to simulate the experimental data.

[DOI: 10.1115/1.2768378]

1 Introduction

The intervertebral disk, is made up of a nucleus, called the nucleus pulposus, which is composed of proteoglycans and type II collagen with a capacity to absorb and distribute load, and an outer annulus, called the annulus fibrosus, which comprises well-organized layers of type I collagen that support the nucleus (Fig. 1). Mechanically, these disks are the flexible joints distributed along the length of an otherwise rigid spine to achieve a stable

flexibility. In Fig. 1, the annulus fibrosus is depicted having alternating statistically dominant fiber directions in adjoining lamellae, which cross each other at an angle of approximately 120 deg [1–3]. Under the effect of vertical loads, the annulus fibrosus is stretched laterally in the direction in which the interfiber angle is 60 deg. These fibers normally exist in wrinkled form in stress-free tissue; as the tensile deformations accumulate, these fibers gradually become straight and the stiffness of the tissue usually increases exponentially. To function properly, the annulus fibrosus, and thus the intervertebral disk, depends on these fibers. Under compression along the fiber direction, on the other hand, the wrinkled fibers cannot contribute to the compressive resistance of the material and thus the material response becomes isotropic.

Stresses well above the average that the tissue can accommo-

¹On leave from School of Civil Engineering, Technical University of Catalonia (UPC), Jordi Girona 1-3, Barcelona, Spain 08034.

Contributed by the Bioengineering Division of ASME for publication in the JOURNAL OF BIOMECHANICAL ENGINEERING. Manuscript received August 16, 2006; final manuscript received February 26, 2007. Review conducted by Ellen M. Arruda.

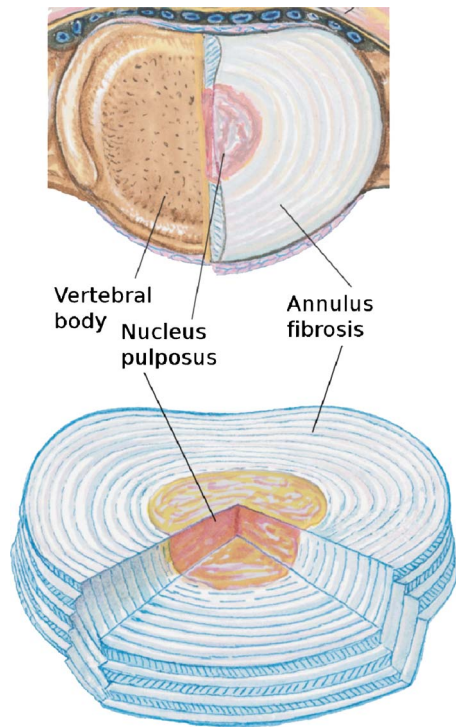


Fig. 1 The top view of intervertebral disk with annulus fibrosus and nucleus pulposus, and oblique view of annulus fibrosus with nucleus pulposus. In the oblique view of annulus fibrosus, its lamellar structure and statistically dominant fiber directions that alternate from one lamella to the other are depicted.

date due to excessive physical activities may cause disorganization of these fibers with time which leads to a degenerated intervertebral disk, the most important etiologic factor for low back pain in mild cases and for the so-called degenerative disk disease (DDD) in the extreme cases [4]. Stresses well above the average can easily happen in daily life during the most ordinary activities if the average stresses are low due to an extreme lack of physical activity because annulus fibrosus undergoes a remodeling so as to be able to accommodate only such small levels of stress. As a result, such diseases are common in modern man mostly due to low levels of activity. Rupture of annulus fibrosus not only results in lower-back pain but also it may result in paralysis in varying degrees depending on the location of the failed disk. Thus, it is essential to have a constitutive model spanning from nonlinearly elastic to inelastic behavior, which finally leads to failure of these lamellae in order to predict the kinetic and kinematic states at failure. Remodeling of the tissue subjected to different types of loads resulting from different physical activities and lifestyles must also be included in the model for accurate predictions of failure state because often the failure is not due to excessive loads but to degenerated collagen structure in the tissue. For example, smoking alone can cause degeneration, or pathological remodeling of collagen fibers in the lamellae, which may result in DDD [5]. Computational results from such realistic constitutive models would provide accurate information about how far each patient is from a determined critical state by comparing numerical (finite element) simulation results with images obtained from a variety of medical imaging devices. Moreover, accurate constitutive modeling is also critical to device efficient artificial disks to treat conditions such as extreme cases of DDD, anterior cervical fusion, and spondylotic cervical myelopathy [6,7].

Experimental observation of material behavior is clearly the most important step in constructing a constitutive model. One of the earliest such studies of annulus fibrosus is Ref. [8] in which its

tensile properties under various loading conditions were reported. In Ref. [9], the incompressibility of annulus fibrosus is established. The size effect on the tensile properties of the annulus fibrosus was studied in Refs. [10,11]. The fiber-matrix interaction was used for the first time in these studies to simulate the tensile stiffness and strength of the annulus fibrosus. In Ref. [12], it was demonstrated that the spatial variations in the tensile properties of the annulus fibrosus resulted from structural variations rather than biochemical differences. The effects of degeneration due to aging on the tensile properties of the annulus fibrosus were reported in Ref. [13], while the spatial variation of tensile properties of healthy annulus fibrosus was reported in Ref. [14]. In Ref. [15], it was shown that the effect of annular collagen fibers with pre-stretch oriented perpendicular to the direction of the applied shear stress on the shear modulus is significant. In Ref. [16], the uniaxial and biaxial tests of the annulus fibrosus were reported. Although the spatial variation of the statistically significant fiber orientation, along with the associated tensile properties, was studied in Ref. [17], the angular fiber distribution at each one of these locations was not reported, which would have been especially relevant for the purposes of this study.

Many of the constitutive laws proposed in literature are based on Spencer's theory of fiber reinforced composites [18,19]. For example, in Ref. [9], a hyperelastic constitutive model in which the strain energy function of this conventional fiber reinforced theory was improved by introducing two new invariants and two families of fibers. By using the parallel coupling model of the fibers and the matrix, an anisotropic hyperelastic fiber reinforced constitutive model for soft tissue was proposed in Ref. [20] and later extended into nonlinear range in Ref. [21]. The use of the model developed in structural analysis of a part of human lumbar spine was demonstrated in Ref. [22]. In Refs. [23,24], a linear anisotropic model for the annulus fibrosus was developed by using a quadratic strain energy function at small strains but involving interlamellar fiber-fiber interaction. The effect of nutrient and electrolyte transport and swelling were accounted for in relatively few studies [25–27]. In Ref. [25], the solid phase (elastin matrix and collagen fibers) was modeled as a hyperelastic composite reinforced with one family of fibers. Unfortunately, the interlamellar fiber-fiber interaction was not accounted for in this model. In Ref. [28], however, the matrix-fiber interaction was accounted for using a separate energy term to this end.

Most hyperelastic anisotropic models for many types of soft tissue published in literature do not account for the fiber distribution. The angular fiber distribution was probably explicitly employed for the first time by Billiar and Sacks [29] in which a structural model for the aortic valve cusp was developed. It was concluded in that study that the fiber distribution was essential to be able to fit biaxial test data of the aortic valve cusp. Sacks later published [30] in which the effect of a 2D angular fiber distribution on the mechanical behavior of biological soft tissue was considered. In that study, a 2D planar constitutive model for collagenous tissue in which the collagen fibers were considered to be fibers with varying "crimp" that begin to carry load when this crimp is removed by progressing deformations was developed. The crimp was modeled using an assumed crimp distribution function, and the in-plane fiber direction distribution was accounted for using a 2D experimentally determined distribution function. The fiber law was assumed to be linear elastic in this case, which is a relatively strong simplification for fiber constitutive behavior. On the other hand, the microplane model presented in this paper (and also microplane model for blood vessel tissue published in Ref. [31]) is a model with nonlinear fiber constitutive law, which can account for experimental fiber distribution in 3D. In Ref. [32], the distribution of fibers in the arterial wall and aortic valves is modeled with a normal probability density function, and the fibers were embedded as structural elements within a finite element mesh. In that study, it was found that the axial prestretch forces were very sensitive to the fiber distribution, and that in

order to be able to fit the biaxial test data, an accurate representation of the fiber distribution was essential, a conclusion shared with Ref. [29]. In Ref. [33], a parameter based on integration of fiber orientation tensor was used to estimate the effect of fiber orientation distribution. Microplane model for blood vessel tissue published in Ref. [31] as well as the microplane model for annulus fibrosus presented in this paper are different from the model in Ref. [32] and also from the models in Refs. [29,30] in that (i) they incorporate the distributed fibers at a zero-sized material point so that the fiber stresses are actually defined at a lower scale than classical macroscale and (ii) they provide homogenization of material response.

Recently two papers, Refs. [34,35], have been submitted for publication in which the fiber-matrix interaction is shown to be indispensable for simulating mechanical behavior of annulus fibrosus by optimally fitting various experimental data from literature and contrasting the results obtained from the model with fiber-matrix interaction against those from the model without any such interaction. The composite model developed in Ref. [35] has been recently examined further both theoretically [36] and numerically [37]. In this study, microplane model for soft tissue published in Ref. [31] is adapted to annulus fibrosus by incorporating two fiber families in accordance with the physiology of the lamellae. To be able to provide a fair comparison, the 1D constitutive law for the fibers is kept the same as in Ref. [34], except for the material parameters, which have to be readjusted because of the 3D angular fiber distribution employed in the microplane model. The constitutive model for the matrix is neo-Hookean in this model as well [31,38]. In contrast, there is no explicit fiber-matrix interaction employed in microplane model for soft tissue. However, there is indeed interaction of distributed fibers provided automatically by construction of the model. Thus, in this study, we show that the microplane model for soft tissue adjusted for human annulus fibrosus can accurately simulate the experimental observations without accounting for an explicit fiber-matrix interaction, because the shear interaction between the individual fibers of the model imagined to represent distributed fibers in the tissue provides the required additional rigidity to explain these experimental facts. Physically, this is equivalent to a combined interlamellar interaction of distributed fibers in different lamellae as well as interaction between the distributed fibers in the same lamella. We note that intensity of the shear interaction between the fibers can be adjusted by adjusting the spread in the distribution while keeping the total amount of fibers constant. Another aspect of microplane model is that the anisotropic effect of the fibers is homogenized due to the volume averaging in the formulation of the model [31,38]. The consequence of averaging is that the anisotropy causing singularities can be represented conveniently in the model. For example, a discrete fiber direction will appear in the microplane model as a Dirac delta function. Thus, the volume averaging inherent in the microplane model admits the interpretation that the microplane stresses are those that belong to a lower scale than the continuum scale, although it is rather difficult to identify this scale precisely.

In this study, we show a comparison of the results obtained from (i) a representative classical anisotropic hyperelastic model with two families of fibers, which does not account for the fiber-matrix interaction [34], (ii) the same model as in (i) but enriched using fiber-matrix interaction [34], and (iii) microplane model for soft tissue adapted to annulus fibrosus with two families of fiber distributions. The conclusions are (i) that varying degrees of fiber-fiber and fiber-matrix shear interaction must be taking place in the human annulus fibrosus, (ii) that this shear interaction is essential to be able to explain the mechanical behavior of human annulus fibrosus, and (iii) the microplane model for soft tissue can be fortified with fiber-matrix interaction in a straightforward manner as in Ref. [34] provided that precise experimental information on fiber distributions across all the lamellae of the annulus fibrosus is

available and that the spread of these distributions is too small so as to require an explicit fiber-matrix interaction to be able to simulate the experimental data.

In the next section, we briefly summarize (i) the classical hyperelastic matrix-fiber parallel coupling model without fiber-matrix interaction and (ii) the same model improved incorporating an explicit fiber-matrix interaction. In the subsequent section, we discuss the microplane model for annulus fibrosus. Next, we show the computational results that simulate the experimental data from literature under various loading conditions and discuss them. Finally, in the last section, we provide the concluding remarks.

2 Hyperelastic Fiber-Matrix Parallel Coupling Model

Peng et al. [34] developed a hyperelastic fiber-matrix parallel coupling model for annulus fibrosus in which fiber-matrix shear interaction is used to be able to simulate the experimental data on annulus fibrosus under various loading conditions. In their model, it is assumed that the strain energy function Ψ is a scalar function of the right Cauchy–Green deformation tensor $\mathbf{C}=\mathbf{F}^T\mathbf{F}$, where \mathbf{F} is the deformation gradient tensor, and the fiber direction in the reference configuration given by \mathbf{a}_0 [19], i.e., $\Psi=\Psi(\mathbf{C},\mathbf{a}_0)$. The elastic response of a single layer of annulus fibrosus is assumed to be made up of the resistance of the matrix, fibers, and their interaction. Accordingly, the strain energy function Ψ can be divided into three parts given by

$$\Psi(\mathbf{C},\mathbf{a}_0)=\Psi^M+\Psi^F+\Psi^{FM} \quad (1)$$

where Ψ^M is the strain energy contribution from the matrix, Ψ^F is the contribution from the fiber stretch, and Ψ^{FM} is the strain energy caused by the fiber-matrix shear interaction. The strain energy function Ψ can be written in terms of principal invariants I_i as

$$\Psi(\mathbf{C},\mathbf{a}_0)=\Psi(I_1,I_2,I_3,I_4,I_5) \quad (2)$$

where

$$\begin{aligned} I_1 &= \text{tr } \mathbf{C} & I_2 &= \frac{1}{2}[(\text{tr } \mathbf{C})^2 - \text{tr } \mathbf{C}^2] \\ I_3 &= \det \mathbf{C} & I_4 &= \mathbf{a}_0 \cdot \mathbf{C} \cdot \mathbf{a}_0 = \lambda_F^2 \\ I_5 &= \mathbf{a}_0 \cdot \mathbf{C}^2 \cdot \mathbf{a}_0 & \lambda_F &= \text{fiber stretch} \end{aligned} \quad (3)$$

The energy Ψ^M stored in the matrix is assumed to be given by that for compressible neo-Hookean material

$$\Psi^M = C_{10}(\bar{I}_1 - 3) + 2D_1^{-1}(J - 1)^2 \quad (4)$$

where $J=\sqrt{I_3}$ is the volume change and $\bar{I}_1=J^{-2/3}I_1$ is the first invariant of the deviatoric right Cauchy–Green strain tensor \mathbf{C}^D ; $C_{10}=\mu_0/2$, where μ_0 is the shear modulus; D_1^{-1} is the bulk modulus. The strain energy for fibers Ψ^F is defined as

$$\Psi^F = C_2\langle I_4 - 1 \rangle^2 + C_3\langle I_4 - 1 \rangle^4 \quad (5)$$

where $\langle x \rangle = \max(x, 0)$ and the symbol $\langle \rangle$ stands for the Macaulay bracket. Thus, it can be inferred from the equation above that when the fiber is under compression, it does not contribute to the resistance of the material; it does so only if it is under tension. Equation (5) leads to the fiber constitutive relation

$$\Sigma^f = 4C_2\langle I_4 - 1 \rangle + 8C_3\langle I_4 - 1 \rangle^3 \quad (6)$$

To model the strain energy contributed by the fiber-matrix interaction, we consider a fiber direction in reference configuration given by \mathbf{a}_0 normal to a surface dS_0 , which deforms into a surface dS with a surface normal given by \mathbf{n} where Nanson's formula [39] can be used to provide the relationship $\mathbf{n}dS = \mathbf{J}\mathbf{a}_0 \cdot \mathbf{F}^{-1}dS_0$. Thus, the normal \mathbf{n} is given by [34]

$$\mathbf{n} = \frac{1}{|\mathbf{a}_0 \cdot \mathbf{F}^{-1}|} \mathbf{a}_0 \cdot \mathbf{F}^{-1} = \frac{1}{\sqrt{\mathbf{a}_0 \cdot \mathbf{C}^{-1} \cdot \mathbf{a}_0}} \mathbf{a}_0 \cdot \mathbf{F}^{-1} \quad (7)$$

On the other hand, the unit fiber direction \mathbf{a}_0 in the reference configuration deforms into the unit fiber direction \mathbf{a} in the current configuration given by [34]

$$\mathbf{a} = \frac{1}{|\mathbf{F} \cdot \mathbf{a}_0|} \mathbf{F} \cdot \mathbf{a}_0 = \frac{1}{|\mathbf{a}_0 \cdot \mathbf{C} \cdot \mathbf{a}_0|} \mathbf{F} \cdot \mathbf{a}_0 \quad (8)$$

and the dot product of the two unit vectors \mathbf{n} and \mathbf{a} furnishes [34]

$$\cos \gamma = \frac{1}{\sqrt{\mathbf{a}_0 \cdot \mathbf{C}^{-1} \cdot \mathbf{a}_0} \lambda_F} \mathbf{a}_0 \cdot \mathbf{F}^{-1} \cdot \mathbf{F} \cdot \mathbf{a}_0 = \frac{1}{\sqrt{I_4(\mathbf{a}_0 \cdot \mathbf{C}^{-1} \cdot \mathbf{a}_0)}} \quad (9)$$

One can express \mathbf{C}^{-1} in terms of powers greater than or equal to zero of itself using the fact that it satisfies its own characteristic equation by virtue of Cayley–Hamilton theorem [40]:

$$\mathbf{C}^{-1} = I_3^{-1}(\mathbf{C}^2 - I_1\mathbf{C} + I_2\mathbf{I}) \quad (10)$$

which, upon substituting into Eq. (9), furnishes

$$\cos \gamma = \mathbf{n} \cdot \mathbf{a} = \sqrt{I_3[(I_5 - I_1I_4 + I_2)I_4]^{-1}} \quad (11)$$

that leads to a new invariant χ^1 , defined as

$$\chi = \tan^2 \gamma = \cos^{-2} \gamma - 1 = I_4 I_3^{-1} (I_5 - I_1 I_4 + I_2) - 1 \quad (12)$$

Now the strain energy function for fiber-matrix interaction can be defined as

$$\Psi^{\text{FM}} = \Psi^{\text{FM}}(I_4, \gamma) = f(I_4) \chi^2 \quad (13)$$

where χ is given by Eq. (12) and $f(I_4)$ is given by [34]

$$f(I_4) = \eta [1 + \exp[-\beta(\lambda_F - \lambda_F^*)]]^{-1} \quad (14)$$

where η is the largest $f(I_4)$ that can be achieved and $f(I_4)$ becomes $\eta/2$ at $\lambda_F = \lambda_F^*$; λ_F^* represents a transitional point in the fiber constitutive law and it must be calibrated to fit the experimental data along with η and β . It must be noted that when $\eta=0$, the fiber-matrix interaction term disappears, making the model equivalent to a classical hyperelastic fiber-matrix parallel coupling model.

Now the constitutive law can be explicitly obtained in terms of second Piola–Kirchhoff stress tensor by taking the derivative of total strain energy Ψ with respect to the Green–Lagrangian strain tensor $\mathbf{E} = (\mathbf{C} - \mathbf{I})/2$, i.e., $\boldsymbol{\Sigma} = \partial\Psi/\partial\mathbf{E} = 2\partial\Psi/\partial\mathbf{C}$. The corresponding Cauchy stress tensor is given by

$$\boldsymbol{\sigma} = \frac{2}{J} \mathbf{F} \cdot \frac{\partial\Psi}{\partial\mathbf{C}} \cdot \mathbf{F}^T = \frac{2}{J} [(I_2\Psi_{,2} + I_3\Psi_{,3})\mathbf{I} + \Psi_{,1}\mathbf{B} - I_3\Psi_{,2}\mathbf{B}^{-1} + I_4\Psi_{,4}\mathbf{a} \otimes \mathbf{a} + I_4\Psi_{,5}(\mathbf{a} \otimes \mathbf{B} \cdot \mathbf{a} + \mathbf{a} \cdot \mathbf{B} \otimes \mathbf{a})] \quad (15)$$

where $\Psi_{,i} = \partial\Psi/\partial I_i$ and $i=1, 2, \dots, 5$; \mathbf{B} is the left Cauchy–Green strain tensor; \mathbf{a} is the fiber direction in the current configuration. If two adjacent lamellae are to be modeled, then assuming that the two distinct fiber directions in the current configuration are given by \mathbf{a}_1 and \mathbf{a}_2 , the Cauchy stress is given by [34]

$$\boldsymbol{\sigma} = \frac{2}{J} \left\{ (I_2\Psi_{,2} + I_3\Psi_{,3})\mathbf{I} + \Psi_{,1}\mathbf{B} - I_3\Psi_{,2}\mathbf{B}^{-1} + \frac{1}{2}(I_{41}\Psi_{,41}\mathbf{a}_1 \otimes \mathbf{a}_1 + I_{42}\Psi_{,42}\mathbf{a}_2 \otimes \mathbf{a}_2) + \frac{1}{2}[I_{41}\Psi_{,51}(\mathbf{a}_1 \otimes \mathbf{B} \cdot \mathbf{a}_1 + \mathbf{a}_1 \cdot \mathbf{B} \otimes \mathbf{a}_1) + I_{42}\Psi_{,52}(\mathbf{a}_2 \otimes \mathbf{B} \cdot \mathbf{a}_2 + \mathbf{a}_2 \cdot \mathbf{B} \otimes \mathbf{a}_2)] \right\} \quad (16)$$

where $I_{4\xi} = (\lambda_F^\xi)^2$; $\Psi_{,i\xi} = \partial\Psi/\partial I_i^\xi$ and $\xi=1, 2$ are the indices of the fiber families; $i=1, 2, \dots, 5$ are the indices of the invariants; $\Psi = \Psi^M + (\Psi_1^F + \Psi_2^F)/2 + (\Psi_1^{\text{FM}} + \Psi_2^{\text{FM}})/2$. It can be inferred that the interaction between the two fiber families is not accounted for in Eq. (16) because the cross terms of type $(\mathbf{a}_1 \otimes \mathbf{a}_2 + \mathbf{a}_2 \otimes \mathbf{a}_1)/2$ are not included.

3 Microplane Constitutive Model for Soft Tissue

Microplane model has been widely used in the constitutive modeling of many different engineering materials for a variety of advantages over other approaches [41–46]. In the case of hyperelastic anisotropic biological soft tissue, (i) it allows introduction of fiber distribution within the material, an experimentally well documented fact [30,32,47], into the model in a straightforward manner; (ii) it facilitates the remodeling studies using the fiber distribution by allowing prediction of change of statistically dominant fiber direction with axially strengthening or weakening fibers; (iii) in the inelastic range, which must be taken into account in the failure prediction of soft tissue at the same time with remodeling of the tissue, it allows the use of many yield surfaces in a consistent manner greatly enhancing the prediction capability. Although remodeling, inelasticity, and thus failure of annulus fibrosus are beyond the scope of this study, we show in this paper that the effect of distribution is significant in predicting the mechanical behavior of annulus fibrosus in the elastic range. In what follows, we first discuss the isotropic neo-Hookean microplane model and subsequently we develop the anisotropic hyperelastic microplane model.

3.1 Isotropic Incompressible Neo-Hookean Microplane Model

The formulation for isotropic compressible neo-Hookean microplane model was developed in Ref. [38]; part of a framework for hyperelastic microplane models and subsequently the anisotropic hyperelastic microplane model for blood vessel tissue was developed in Ref. [31]. In these formulations, the macroscopic free energy per unit volume, denoted $\rho_0\Psi$, is assumed to be integral of microplane free energies per unit area of a unit hemisphere Ψ_Ω , i.e.,

$$\frac{2\pi R^3}{3} \rho_0\Psi = \int_\Omega \Psi_\Omega d\Omega \quad (17)$$

Here, $R=1$ is the radius of the unit hemisphere, Ω denotes the surface of the unit hemisphere, ρ_0 is the mass density, Ψ is the macroscopic free energy per unit mass per unit volume, and Ψ_Ω is the microplane free energy per unit area given by

$$\Psi_\Omega(\lambda_D, \lambda_J) = \mu_0 \left(\frac{\lambda_D^2}{2} + \frac{\lambda_D^{-3}}{3} - \frac{5}{6} \right) + \frac{1}{3} g(J) \quad (18)$$

In this equation, μ_0 is the material constant, λ_D is distortional stretch, $J = \det \mathbf{F}$ is the volume change with $\mathbf{F} = \partial\mathbf{x}/\partial\mathbf{X}$ being the deformation gradient tensor, and $g(J)$ is the volumetric energy function. The microplane stretch is defined as

$$\lambda_N = \lambda_D \lambda_J = \sqrt{\mathbf{N} \cdot \mathbf{C} \cdot \mathbf{N}} \quad (19)$$

where $\lambda_J = J^{1/3}$ is the volumetric stretch, \mathbf{N} is the microplane normal vector, and \mathbf{C} is the right Cauchy–Green tensor. The volumetric energy function must satisfy the conditions

$$g|_{J=1} = 0 \quad \text{and} \quad \left. \frac{dg}{dJ} \right|_{J=1} = 0 \quad (20)$$

so that in the undeformed state (when $J=1$ and $\lambda_D=1$) the potential vanishes. Obviously, it is possible to find many such volumetric functions. Examples of popular functions used in the literature are $g(J) = \lambda_0(\ln J)^2/2 - \mu_0(\ln J)$ (e.g., Ref. [48]) and $g(J) = \lambda_0(J-1)^2/2$ (e.g., Refs. [21,49–52]), where λ_0 is the bulk modulus (fictitious bulk modulus or the penalty parameter when incompressibility is enforced). In this work, one of the simplest forms given by

$$g(J) = \frac{\lambda_0}{2} \left(J + \frac{1}{J} - 2 \right) \quad (21)$$

which also satisfies the conditions given in Eqs. (20) is used [38].

It can be shown that substitution of Eqs. (18), (19), and (21) into Eq. (17) results in

$$\rho_0 \Psi = \frac{\mu_0}{2} (I_1^D - 3) + g(J) \quad (22)$$

where I_1^D is the first invariant of \mathbf{C}^D , the distortional right Cauchy–Green tensor given by $\mathbf{C}^D = J^{-2/3} \mathbf{C}$. Clearly, Eq. (22) is the equation of free energy per unit volume of a neo-Hookean solid [40].

The constitutive relation can be obtained in view of either Eq. (22) in closed form or Eq. (17) in integral form. Noting $\partial J / \partial \mathbf{E} = J \mathbf{C}^{-1}$ and $\partial I_1 / \partial \mathbf{E} = 2 \mathbf{I}$ [38], in view of Eq. (22), one obtains

$$\boldsymbol{\Sigma} = \frac{\partial(\rho_0 \Psi)}{\partial \mathbf{E}} = \mu_0 J^{-2/3} \left[\mathbf{I} - \frac{I_1^D}{3} (\mathbf{C}^D)^{-1} \right] + \frac{\lambda_0}{2} (J^{5/3} - J^{-1/3}) (\mathbf{C}^D)^{-1} \quad (23)$$

where \mathbf{I} denotes the second order identity tensor. In view of Eq. (17), the integral form

$$\begin{aligned} \boldsymbol{\Sigma} &= \frac{\partial(\rho_0 \Psi)}{\partial \mathbf{E}} = \frac{3}{2\pi} \int_{\Omega} \left(\frac{\partial \Psi_{\Omega}}{\partial \lambda_D} \frac{\partial \lambda_D}{\partial \mathbf{E}} + \frac{\partial \Psi_{\Omega}}{\partial \lambda_J} \frac{\partial \lambda_J}{\partial \mathbf{E}} \right) d\Omega \\ &= \frac{3}{2\pi} \int_{\Omega} \left(\Sigma_D \frac{\partial \lambda_D}{\partial \mathbf{E}} + \Sigma_J \frac{\partial \lambda_J}{\partial \mathbf{E}} \right) d\Omega \end{aligned} \quad (24)$$

where $\boldsymbol{\Sigma}$ is the macroscopic second Piola–Kirchhoff (PK) stress tensor and \mathbf{E} is the Green–Lagrangian strain tensor, is obtained. In view of Eqs. (18) and (21), the microplane stresses Σ_D and Σ_J are calculated as

$$\begin{aligned} \Sigma_D &= \frac{\partial \Psi_{\Omega}}{\partial \lambda_D} = \mu_0 (\lambda_D - \lambda_D^{-4}) \\ \Sigma_J &= \frac{\partial \Psi_{\Omega}}{\partial \lambda_J} = \frac{\lambda_0}{2} (\lambda_J^2 - \lambda_J^{-4}) \end{aligned} \quad (25)$$

In order to be able to evaluate the integral in Eq. (24), we note that [38]

$$\frac{\partial \lambda_D}{\partial \mathbf{E}} = \lambda_D^{-1} \lambda_J^{-2} \mathbf{N} \otimes \mathbf{N} - \frac{1}{3} \lambda_D \mathbf{C}^{-1}$$

Finally, substituting Eq. (25) and Eqs. (26) into Eq. (24), one obtains the relationship between macroscopic second PK stress tensor and the microplane second PK stresses as

$$\begin{aligned} \boldsymbol{\Sigma} &= \frac{3}{2\pi} \int_{\Omega} \left[\Sigma_D \left(\frac{1}{\lambda_D \lambda_J^2} \mathbf{N} \otimes \mathbf{N} - \frac{1}{3} \lambda_D \mathbf{C}^{-1} \right) + \Sigma_J \frac{\lambda_J}{3} \mathbf{C}^{-1} \right] d\Omega \\ &= \frac{3}{2\pi} \int_{\Omega} \left[\Sigma_D \left(\frac{1}{\lambda_D \lambda_J^2} \mathbf{N} \otimes \mathbf{N} - \frac{1}{3} \lambda_D \mathbf{C}^{-1} \right) \right] d\Omega + \Sigma_J \lambda_J \mathbf{C}^{-1} \end{aligned} \quad (26)$$

It can be shown that Eqs. (26) and (23) are the same by substituting the identities $3/(2\pi) \int_{\Omega} \mathbf{N} \otimes \mathbf{N} d\Omega = \mathbf{I}$, $3/(2\pi) \int_{\Omega} \lambda_D^2 d\Omega = I_1 J^{-2/3}$, $3/(2\pi) \int_{\Omega} \lambda_D^{-5} / \lambda_J^2 \mathbf{N} \otimes \mathbf{N} d\Omega = \mathbf{C}^{-1}$, $3/(2\pi) \int_{\Omega} \lambda_D^{-3} / 3 d\Omega = 1$, and Eqs. (25) into Eq. (26) [38].

3.2 Collagen Fibers: Anisotropic Microplane Model. Anisotropy due to collagen fibers within the tissue has usually been formulated by introducing a few dominant fiber directions within the tissue as done in Ref. [20], where the behavior of crimped and fully straightened fibers is represented by the initial and final parts, respectively, of the exponential fiber law.

Introduction of generalized anisotropy as in the sense of orthotropic polymer composites into the microplane formulation, which is beyond the scope of this work, can be achieved using a spectral decomposition of orthotropic stiffness matrix [53]. For modeling nearly incompressible soft tissue, introduction of generalized anisotropy into the microplane formulation can be achieved by including an anisotropy function, $\phi(\mathbf{N})$, in the integral over the microplanes [31]. In general, the form of anisotropy described by

the anisotropy function $\phi(\mathbf{N})$ can vary from no anisotropy to strong anisotropy. In the former case, $\phi(\mathbf{N}) = 1/3$, so that $3/(2\pi) \int_{\Omega} \phi(\mathbf{N}) d\Omega = 1$. In the latter case, this function can become $\phi(\mathbf{N}) = [\delta(\mathbf{N}, \mathbf{N}^{(1)}) + \delta(\mathbf{N}, \mathbf{N}^{(2)}) + \delta(\mathbf{N}, \mathbf{N}^{(3)}) + \dots] 2\pi/3$, where the directions $\mathbf{N}^{(1)}, \mathbf{N}^{(2)}, \mathbf{N}^{(3)}, \dots$ are fiber (or strong anisotropy) directions and $\delta(\mathbf{N}, \mathbf{N}^{(l)})$ are Dirac delta functions. The coefficient $2\pi/3$ is determined from the condition that all $\phi(\mathbf{N})$ must satisfy

$$\frac{3}{2\pi} \int_{\Omega} \phi(\mathbf{N}) d\Omega = 1 \quad (27)$$

in order to be able to treat $\phi(\mathbf{N})$ as a probability density function.

For example, to introduce a single direction of anisotropy due to a family of fibers in direction $\mathbf{N}^{(1)}$ (a transversely isotropic solid), one can simply introduce $\phi(\mathbf{N}) = \delta[\mathbf{N}, \mathbf{N}^{(1)}] 2\pi/3$ into the integrand yielding

$$\begin{aligned} \boldsymbol{\Sigma}^{f(1)} &= \frac{3}{2\pi} \int_{\Omega} \phi(\mathbf{N}) \boldsymbol{\Sigma}^f \mathbf{N} \otimes \mathbf{N} d\Omega = \int_{\Omega} \delta[\mathbf{N}, \mathbf{N}^{(1)}] \boldsymbol{\Sigma}^f \mathbf{N} \otimes \mathbf{N} d\Omega \\ &= \boldsymbol{\Sigma}^{f(1)} \mathbf{N}^{(1)} \otimes \mathbf{N}^{(1)} \end{aligned} \quad (28)$$

Typically, the matrix is modeled as a neo-Hookean material as in Refs. [20,21,24]. In such models, the soft tissue is modeled as a neo-Hookean solid with a given pair of discrete fiber directions, which are determined statistically from an experimentally obtained distribution of fiber directions. In these models, if there are n_f number of distinct fiber families (directions) in the material, and the response of the matrix is given by the neo-Hookean constitutive law, the total stress may be obtained as

$$\boldsymbol{\Sigma} = \mu_0 J^{-2/3} \left[\mathbf{I} - \frac{I_1^D}{3} (\mathbf{C}^D)^{-1} \right] + J^{1/3} g'(J) (\mathbf{C}^D)^{-1} + \sum_{l=1}^{n_f} \boldsymbol{\Sigma}^{f(l)} \quad (29)$$

where $\boldsymbol{\Sigma}^{f(l)}$ are given by Eq. (28) if all superscripts (1) are replaced by (l). Incompressibility could then be imposed on the total potential from which stress $\boldsymbol{\Sigma}$ above is derived.

However, it is often impossible to account for each and every fiber direction using discrete representations if the material inherently exhibits a range of fiber directions. In that case, it is much more convenient to treat $\phi(\mathbf{N})$ as a probability density function that represents the fiber direction distribution in the material. In Ref. [47], it is already reported that under a microscopic study of arterial tissue, a directional distribution of densely packed collagen structures is observed. Similar observations were made for aortic valves [32]. The probability density function corresponding to the distribution of orientation of cell nuclei (and thus that of the collagen fibers) in a human aortic media in 2D reported in Ref. [47] is given in Fig. 2. To facilitate the computations, the discrete data points are fitted with a convenient probability density function given by

$$\phi(\mathbf{N}) = \Phi(\theta) = c_1 \exp(c_2 \theta^2) \quad (30)$$

where θ is the angle in radians measured from the circumferential direction. The optimum fit to the experimental data points is obtained for $c_1 = 3.74$ and $c_2 = -11.0$, for which $\int_0^{\pi/2} \Phi(\theta) d\theta \approx 1$. In Ref. [3], this distribution is extended to 3D by treating it as an azimuthal distribution with respect to material coordinates, and thus in 3D the aortic media are assumed to be anisotropic axisymmetrically about the circumferential direction passing through the middle of media. Then, the function is scaled so that $3/(2\pi) \int_0^{\pi/2} \int_0^{2\pi} \Phi(\theta) \sin \theta d\alpha d\theta \approx 1$, which yields $c_1 = 7.43$. It must be noted that this assumption may be replaced with the actual 3D distribution of collagen fibers if the relevant experimental data could be obtained. For annulus fibrosus, we assume a narrower distribution (i.e., a distribution with less spread) that corresponds to $c_2 = -60$ and $c_1 = 18.5$ results if the area under the curve is kept

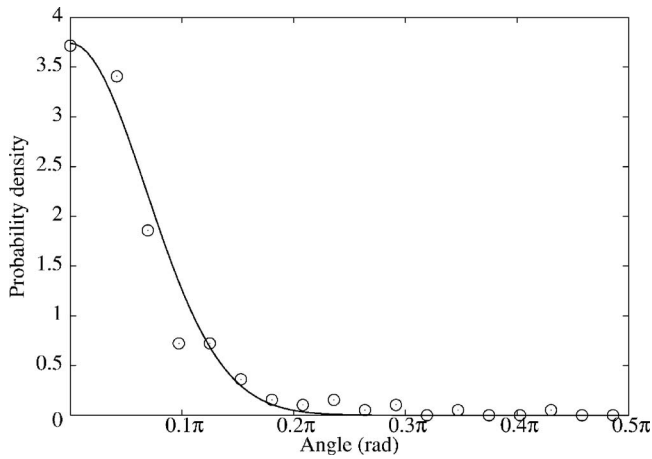


Fig. 2 The distribution of orientation of cell nuclei (and thus of collagen fibers) in aortic media (taken from Ref. [47]) shown with circles, and the associated best fit probability density function

constant. Note that this distribution has a profound effect on the behavior of the resulting model. For example, if a very narrow distribution in which the total amount fiber is kept constant were used, the model would behave like a hyperelastic model with discrete structural fibers.

Thus, the proposed microplane constitutive law with a continuous representation of fiber directions in 3D can be expressed as

$$\Sigma = \frac{3}{2\pi} \int_{\Omega} \left\{ \left[\frac{\Sigma_D}{\lambda_D \lambda_J^2} + \phi(\mathbf{N}) \Sigma^f \right] \mathbf{N} \otimes \mathbf{N} - \Sigma_D \frac{1}{3} \lambda_D \mathbf{C}^{-1} \right\} d\Omega + \Sigma_J \lambda_J \mathbf{C}^{-1} \quad (31)$$

where the fiber constitutive law is given by Eq. (6). It must be noted that the way many fiber families aligned in different directions are treated in Eq. (31) is very different than that in Eq. (29). In the former, the effect of the fibers is homogenized within a material point, whereas in the latter the homogenization can take place only at the finite element level. Consequently, in the former, the fibers are embedded in a zero-sized material point with fiber stresses being defined at a lower scale than the classical macroscale and in the latter, the fibers are treated as structural components in a finite element mesh with fiber stresses being at the classical macroscale. In the former case, the fiber stresses are carried over to the classical macroscale through homogenization integral over a representative unit hemisphere.

Equation (31) is valid for the general case of the compressible material. To get the corresponding constitutive law for incompressible materials, one can impose the incompressibility condition $J=1$ on this equation. It must be noted that, in view of Eq. (31), (i) the probability density function $\phi(\mathbf{N})$ could also be interpreted as the fiber volume fractions (i.e., ratio of the volume of fibers in a given direction to total fiber volume) as a function of direction; (ii) furthermore, it is physically possible to imagine the material point as a microplane system where each microplane embeds a circular fiber in the direction of its normal whose radius (or thickness) is determined by the function $\phi(\mathbf{N})$.

The integral in Eq. (31) is evaluated numerically using Gaussian quadrature rule [54,55] as follows:

$$\Sigma - \Sigma_J \lambda_J \mathbf{C}^{-1} = \frac{3}{2\pi} \int_{\Omega} s d\Omega \approx 6 \sum_{n=1}^{N_m} \omega^{(n)} s^{(n)}$$

where

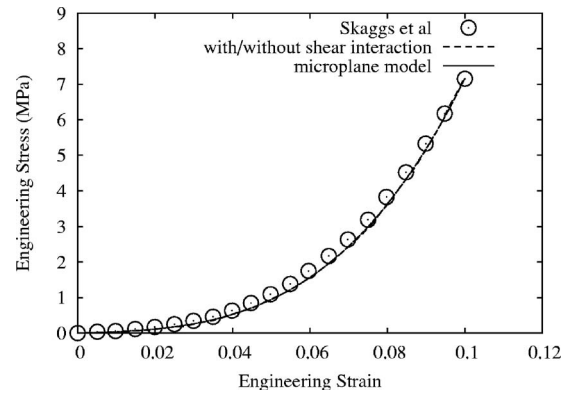


Fig. 3 Tensile stress-strain behavior of single layer human anterior outer annulus fibrosus along the fiber direction

$$s^{(n)} = \left[\frac{\Sigma_D^{(n)}}{\lambda_D^{(n)} \lambda_J^2} + \phi^{(n)} \Sigma^f \right] \mathbf{N}^{(n)} \otimes \mathbf{N}^{(n)} - \frac{\Sigma_D^{(n)}}{3} \lambda_D^{(n)} \mathbf{C}^{-1} \quad (32)$$

where $\omega^{(n)}$ is the weight associated with the n th quadrature point (or n th microplane) and N_m is the total number of quadrature points (or microplanes). In this equation, the quantities with the superscript (n) are those evaluated at the n th quadrature point (or at the n th microplane).

4 Results and Discussion

The predicted mechanical responses from three different constitutive laws, namely, fiber-matrix parallel coupling model *without* shear interaction between the fibers and matrix, fiber-matrix parallel coupling model *with* shear interaction between the fibers and matrix, and microplane model for annulus fibrosus, are demonstrated in Figs. 3–8. In each figure, the relevant experimental data are plotted using symbols, and numerical predictions are plotted using lines; the dashed line is used for plotting the response from fiber-matrix parallel coupling model without shear interaction between the fibers and matrix, the dash-dotted line is used for plotting the prediction from fiber-matrix parallel coupling model with shear interaction between the fibers and matrix, and the solid curve is used for plotting the response from microplane model for annulus fibrosus, as shown in the legend of each figure.

In Fig. 3, the fits for all three models are shown, although there appears to be only one curve present. The experimental data shown in this figure are fitted first in the calibration of all three models. The responses by the fiber-matrix parallel coupling models with and without shear interaction between the fibers and ma-

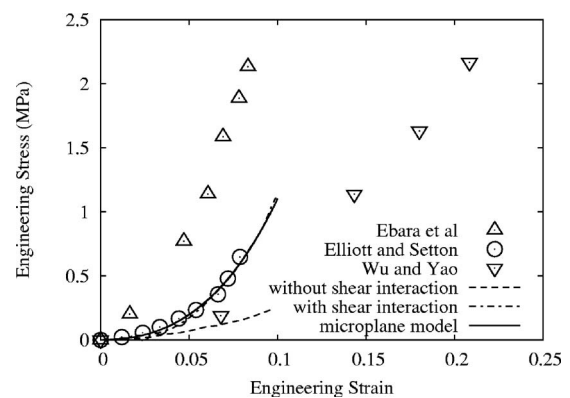


Fig. 4 Tensile stress-strain behavior of multi-layer human anterior outer annulus fibrosus; interfiber angle facing the loading direction is 60 deg

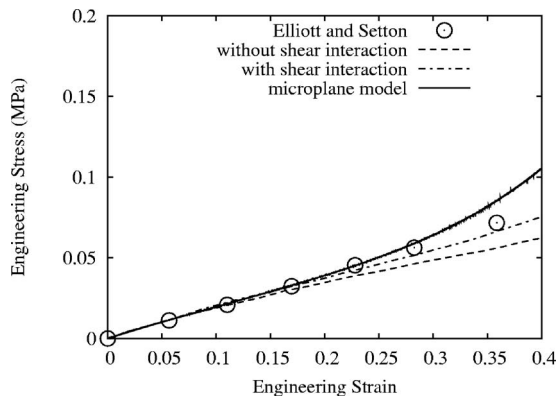


Fig. 5 Tensile stress-strain behavior of multilayer human anterior outer annulus fibrosus; interfiber angle facing the loading direction is 120 deg

trix were obtained using $C_{10}=0.034$ MPa, $D_1=0.197$ MPa⁻¹ for simulating the neo-Hookean matrix behavior and the incompressibility; $C_2=0.45$ MPa, $C_3=82.6$ MPa of the fiber law are determined from optimally fitting these data. As shown, all three curves coincide; therefore, all three models provide the same, nearly perfect simulation of the test data. Note that, by fitting only these data, the fiber-matrix parallel coupling model without shear interaction is calibrated fully, i.e., there is no other free material parameter to calibrate using other test data.

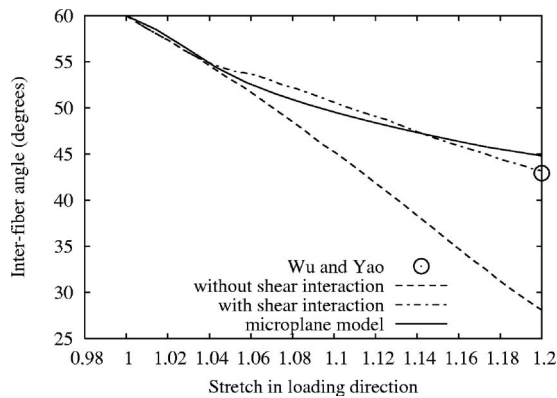


Fig. 6 Interfiber angle change against stretch in the loading direction in multilayer human anterior outer annulus fibrosus; interfiber angle facing the loading direction is 60 deg

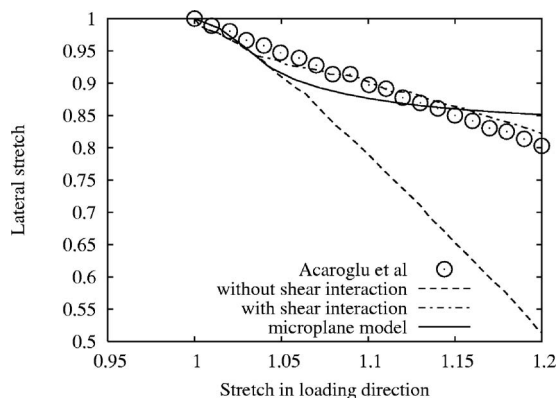


Fig. 7 Stretch in the lateral direction against stretch in the loading direction in multilayer human anterior outer annulus fibrosus; interfiber angle facing the loading direction is 60 deg

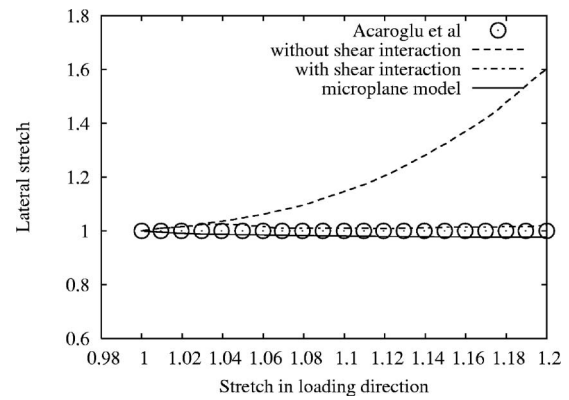


Fig. 8 Stretch in the through-thickness direction against stretch in the loading direction in multilayer human anterior outer annulus fibrosus; interfiber angle facing the loading direction is 60 deg

In Fig. 4, the experimental data from several researchers in the form of engineering stress against engineering strain in the direction of loading of annulus fibrosus with an interfiber angle of 60 deg facing the loading direction are plotted. The plot shows that the material properties of annulus fibrosus show significant differences; these differences are likely to be linked to factors such as age, lifestyle, and diseases of the individuals from which the test samples are taken. In this study, we chose to fit the one by Elliott and Setton [24], because they also provide equivalent data in the perpendicular direction, as shown in Fig. 5. Fitting both of these data is required for any constitutive law. The parameters $\eta = 12$ MPa, $\beta=125$, and $\lambda_F^*=1.02$ of the parallel coupling model with fiber-matrix interaction are obtained by simultaneously fitting both of the test data appearing in Figs. 4 and 5. As a result, the fiber-matrix parallel coupling model with fiber-matrix interaction is calibrated fully, i.e., the parameters of this model are kept constant in the simulation of all other test data shown in Figs. 6–8.

The calibration process for microplane model is similar, but the material parameters are fewer because there is no explicit fiber-matrix interaction considered. Including such a formulation is rather straightforward and it is left for future work. In the microplane model, the material parameters $\mu_0=2C_{10}=0.068$ MPa, the matrix shear stiffness, and the parameters of the fiber law $C_1=6.0$ MPa and $C_2=5000.0$ MPa are obtained by fitting the test data in Fig. 4. The parameters appearing in the fiber distribution law, $c_1=18.5$ and $c_2=-60.0$, are obtained by simultaneously fitting Figs. 4 and 5. In the calculations with microplane model, incompressibility is enforced using a penalty parameter updated as the deformations accumulate; however, in some cases at the extreme end of the simulations, deviations from incompressibility are noted. As such, the deviations at the extreme end of the curves in Figs. 5–7 are due to the penalty parameter not being able to satisfy the incompressibility constraint once the stretches grow very large. The reason for having difficulties in satisfying the incompressibility constraint at large stretches is that the fibers of annulus fibrosus are too rigid at large stretches. For example, in simulating the behavior of blood vessels, the existing penalty algorithm had provided more accurate results in terms of imposing incompressibility. However, such an outcome is expected due to the use of fiber distribution in the microplane model which would cause the model to lock in the limit as the fiber rigidity becomes very large. In contrast, the parallel coupling models will not be locked under the same conditions because discrete rigid fibers will form a mechanism which will still accommodate deformations.

Since the test data in Fig. 4 are used to calibrate the two models, namely, the fiber-matrix parallel coupling model with fiber-matrix shear interaction and the microplane model for annulus fibrosus, the simulations provided by these two models are very

good; in fact, the one by microplane model is slightly better. However, the dashed curve indicates that the fiber-matrix parallel coupling model without fiber-shear interaction is unable to simulate the behavior of the material under this particular loading conditions. In fact, this response may be considered even beyond the spread in the experimental data available in the literature.

Figure 5 depicts engineering stress against engineering strain with two family of fibers aligned at 120 deg, i.e., lateral to the direction of loading to which the material response is shown in Fig. 4. This figure is a figure in which all three models must predict the data. Microplane model performs quite well in this simulation, and the worst performer is the parallel coupling model without shear interaction. However, considering the spread in the data, all these simulations may seem reasonable. The upward trend shown in the response of the microplane model at large stretch is due to difficulties in enforcing incompressibility at such large stretches.

There is only one data point shown in Fig. 6, which depicts variation of interfiber angle with stretch in the loading direction. In this figure, microplane model performs very well despite the fact that it does not have the explicit formulation for interaction. The parallel coupling model with shear interaction also performs very well, but the performance of that without the shear interaction might not be considered acceptable.

Figure 7 shows the lateral stretch (not the through-thickness stretch, but the other one) against stretch in the loading direction. The best performer in this figure is the parallel coupling model with shear interaction, and the worst performer is that without shear interaction. The result obtained in this figure using microplane model is probably due to inaccuracies resulting from a loose enforcement of incompressibility that resulted at large stretches. However, the prediction of microplane model in this figure is quite close to that of the parallel coupling model with shear interaction.

In Fig. 8 in which the lateral through thickness stretch is plotted against loading direction stretch, microplane model performs as good as parallel coupling model with shear interaction, that without the interaction performs probably beyond the acceptable limits.

5 Conclusions

Three models for the mechanical behavior of annulus fibrosus, namely, fiber-matrix parallel coupling model, fiber-matrix parallel coupling model with fiber-matrix shear interaction, and microplane model for soft tissue adjusted for the annulus fibrosus, are compared against experimental data available in the literature and against each other. The microplane model for soft tissue does not contain any explicit formulation for shear interaction. However, the construction of the model allows such an interaction to take place between the fibers at material point level because of homogenization provided by the averaging over a unit hemisphere. In contrast, when the same distribution is included with fibers as macroscopic structural components, the homogenization could take place only at the finite element level. Physically, this is equivalent to a combined interlamellar interaction of distributed fibers in different lamellae as well as interaction between the distributed fibers in the same lamella. We note that intensity of the shear interaction between the fibers can be adjusted by adjusting the spread in the distribution while keeping the total amount of fibers constant. Another aspect of microplane model is that the anisotropic effect of the fibers is homogenized due to the volume averaging in the formulation of the model [31,38]. The consequence of averaging is that the anisotropy causing singularities can be represented conveniently in the model. For example, a discrete fiber direction will appear in the microplane model as a Dirac delta function. Thus, the volume averaging inherent in the microplane model admits the interpretation that the microplane stresses are those that belong to a lower scale than the continuum scale, although it is rather difficult to identify this scale precisely.

It is clear that the parallel coupling model performs very well in all the simulations, and it is equally clear that without shear interaction, this model cannot be reliably used for the mechanics of outer annulus fibrosus. Microplane model, on the other hand, is shown to perform very well in all of these simulations, despite the fact that an explicit fiber-matrix interaction is not employed in the model. At very large stretches, the incompressibility condition was observed to be difficult to satisfy using microplane model due to very stiff fibers in the annulus fibrosus (for example, at even larger deformations, no problems were observed in the mechanics of blood vessels in which the fibers are typically an order of magnitude less rigid).

The behavior of microplane model for annulus fibrosus can be adjusted by adjusting the spread in the fiber distribution keeping the area under the distribution constant (Fig. 2). For example, when the spread drops too much (i.e., when $c_2 < -100$), the fits in Figs. 6–8 are affected in such a way that the response approaches that predicted by the parallel coupling model without shear interaction. Thus, in the formulation of microplane model, the angular fiber distribution would compete against an explicit fiber-matrix interaction. If experimental data were available indicating a common incidence of a particular angular fiber distribution, the parameters of the distribution could no longer be used in data fitting, and to be able to fit the test data, an explicit fiber-matrix interaction would have to be introduced.

At this point, it is also opportune to review other favorable properties of microplane model for soft tissue that is not immediately clear from what we have discussed so far. With microplane model, (1) the inelastic behavior of soft tissue could be modeled in the sense of multisurface plasticity but with an enormously large number of yield surfaces (because each microplane could be associated with a yield surface) that help fine-tune the inelastic response and still ensure a smooth computational response, and (2) the stretch induced remodeling of soft tissue could be achieved assuming only a fiber strengthening law by which the evolution of dominant fiber direction can be computed as opposed to classical models in which a law, in addition to the fiber strengthening law, that prescribes the evolution of dominant fiber direction must also be assumed.

The fibers could in principle be handled separately from the microplane system, as in the model of Holzapfel [47], but in addressing the changes in the orientation of fibers as a result of remodeling such an approach could have shortcomings. One problem in such an approach may be that the remodeling law would have to account for not only the strengthening (or weakening) of fibers but also the change in the statistical mean of their orientation. In microplane approach, it is possible to calculate the change in the statistical mean of orientation by using rather simple laws for individual fiber strengthening (or weakening). For example, one may postulate a simple strengthening of previously weak fibers now aligned in the direction of loading, and the change in the statistical mean of the fiber direction could now be calculated instead of assuming a law that prescribes it. Microplane model in general decomposes the problem of determination of material behavior into that of the constituents of the material thereby reducing the complexity of the assumed material laws for the constituents at the same time increasing the predictive capabilities of the resulting material law.

In Ref. [56], collagen remodeling is simulated and its effects on mechanical properties of the material as a function of individual fiber stretches and fiber volume ratios in aortic valves are discussed. From the point of view of microplane model, this means the microplane stress-stretch laws being modified with stretch and fiber volume ratio on that microplane. In Ref. [57], the effect of cell orientation in bioartificial tissue with fibroblast populated collagen vessels is investigated. To model such behavior using microplane model, the anisotropy caused by changes in cell orientation can be easily reflected in the function $\phi(\mathbf{N})$. Healing of the wounds also result in remodeling of the new tissue: In Ref. [58], it

is suggested that while ligaments and tendons heal, the cells are not aligned with the normal orientation (of the undamaged tissue) and collagen matrix is not organized as in normal (undamaged) tissues. In blood vessels, a transplant operation, therefore, is likely to change the orientation of cells and collagen/elastin fibers in the vicinity of the operated part. An accurate stress analysis of such tissues require the anisotropy, which is not necessarily the same as the surrounding tissue, to be taken into account. Thus, microplane model is a very promising model for description of both stationary and evolving anisotropies in various biological tissues.

Lastly, when compared to classical tensorial models, the only disadvantage of microplane model is increased computational effort required in the analyses. However, hierarchical multiscale models that operate at multiple scales but at much higher computational costs may outperform microplane model. Thus, microplane model can be considered as a compromise between powerful but computationally expensive hierarchical multiscale constitutive models and classical constitutive models based on tensorial invariants.

References

- [1] White, A. A., and Panjabi, M. M., 1990, *Clinical Biomechanics of the Spine*, Lippincott Williams & Wilkins, New York.
- [2] Cassidy, J. J., Hiltner, A., and Baer, E., 1989, "Hierarchical Structure of the Intervertebral Disk," *Connect. Tissue Res.*, **23**, pp. 75–88.
- [3] Hickey, D. S., and Hukins, D. W. L., 1980, "X-Ray Diffraction Studies of the Arrangement of Collagenous Fibers in Human Fetal Intervertebral Disc," *J. Anat.*, **131**, pp. 81–90.
- [4] Stokes, I. A., and Iatridis, J. C., 2004, "Mechanical Conditions That Accelerate Intervertebral Disc Degeneration: Overload vs. Immobilization," *Spine*, **29**(23), pp. 2724–2732.
- [5] Oda, H., Matsuzaki, H., Tokuhashi, Y., Wakabayashi, K., Uematsu, Y., and Iwahashi, M., 2004, "Degeneration of Intervertebral Discs Due to Smoking: Experimental Assessment in a Rat-Smoking Model," *J. Orthop. Sci.*, **9**(2), pp. 135–141.
- [6] Matge, G., 1998, "Anterior Interbody Fusion With the BAK-Cage in Cervical Spondylosis," *Acta Neurochir.*, **140**(1), pp. 1–8.
- [7] Sekhon, L. H. S., 2004, "Two-Level Artificial Disc Placement for Spondylotic Cervical Myelopathy," *J. Neuropsychiatry Clin. Neurosci.*, **11**(4), pp. 412–415.
- [8] Galante, J. O., 1967, "Tensile Properties of the Human Lumbar Annulus Fibrosus," *Acta Orthop. Scand. Suppl.*, **100**, pp. 4–91.
- [9] Wu, H. C., and Yao, R. F., 1976, "Mechanical Behavior of the Human Annulus Fibrosus," *ASME J. Biomech. Eng.*, **9**, pp. 1–7.
- [10] Adams, M. A., and Green, T. P., 1993, "Tensile Properties of the Annulus Fibrosus: I. The Contribution of Fiber-Matrix Interactions to Tensile Stiffness and Strength," *Eur. Spine J.*, **2**, pp. 203–208.
- [11] Green, T. P., Adams, M. A., and Dolan, P., 1993, "Tensile Properties of the Annulus Fibrosus: II. Ultimate Tensile Strength and Fatigue Life," *Eur. Spine J.*, **2**, pp. 209–214.
- [12] Skaggs, D. L., Weidenbaum, M., Iatridis, J. C., Ratcliffe, A., and Mow, V. C., 1994, "Regional Variation in Tensile Properties and Biochemical Composition of the Human Lumbar Annulus Fibrosus," *Spine*, **19**, pp. 1310–1319.
- [13] Acaroglu, E. R., Iatridis, J. C., Setton, L. A., Foster, R. J., Mow, V. C., and Weidenbaum, M., 1995, "Degeneration and Aging Affect the Tensile Behavior of Human Lumbar Annulus Fibrosus," *Spine*, **20**, pp. 2690–2701.
- [14] Ebara, S., Iatridis, J. C., Setton, L. A., Foster, R. J., Mow, V. C., and Weidenbaum, M., 1996, "Tensile Properties of Nondegenerate Human Lumbar Annulus Fibrosus," *Spine*, **21**, pp. 452–461.
- [15] Fujita, Y., Wagner, D. R., Biviji, A. A., Duncan, N. A., and Lotz, J. C., 2000, "Anisotropic Shear Behavior of the Annulus Fibrosus: Effect of Harvest Site and Tissue Prestrain," *Med. Eng. Phys.*, **22**, pp. 349–357.
- [16] Bass, E. C., Ashford, F. A., Segal, M. R., and Lotz, J. C., 2004, "Biaxial Testing of Human Annulus Fibrosus and its Implications for a Constitutive Formulation," *Ann. Biomed. Eng.*, **32**, pp. 1231–1242.
- [17] Holzapfel, G. A., Schulze-Bauer, C. A. J., Feigl, G., and Regitnig, P., 2005, "Single Lamellar Mechanics of the Human Lumbar Annulus Fibrosus," *Biomechanics and Modeling in Mechanobiology*, **3**(3), pp. 125–140.
- [18] Spencer, A. J. M., 1972, *Deformations of Fiber-Reinforced Materials*, Oxford Science Research Papers, New York.
- [19] Spencer, A. J. M., 1984, *Continuum Theory of the Mechanics of Fiber-Reinforced Composites*, Springer, New York.
- [20] Holzapfel, G. A., Gasser, T. C., and Ogden, R. W., 2000, "A New Constitutive Framework for Arterial Wall Mechanics and a Comparative Study of Material Models," *J. Elast.*, **61**, pp. 1–48.
- [21] Gasser, T. C., and Holzapfel, G. A., 2002, "A Rate-Independent Elastoplastic Constitutive Model for Biological Fiber-Reinforced Composites at Finite Strains: Continuum Basis, Algorithmic Formulation and Finite Element Implementation," *Comput. Mech.*, **29**, pp. 340–360.
- [22] Eberlein, R., Holzapfel, G. A., and Fröhlich, M., 2004, "Multi-Segment FEA of the Human Lumbar Spine Including the Heterogeneity of the Annulus Fibrosus," *Comput. Mech.*, **34**, pp. 147–163.
- [23] Elliott, D. M., and Setton, L. A., 2000, "A Linear Material Model for Fiber-Induced Anisotropy of the Annulus Fibrosus," *ASME J. Biomech. Eng.*, **122**, pp. 173–179.
- [24] Elliott, D. M., and Setton, L. A., 2001, "Anisotropic and Inhomogeneous Tensile Behavior of the Human Annulus Fibrosus: Experiments Measurement and Material Model Predictions," *ASME J. Biomech. Eng.*, **123**, pp. 256–263.
- [25] Sun, D. N., and Leong, K. W., 2004, "A Nonlinear Hyperelastic Mixture Theory for Anisotropy, Transport, and Swelling of Annulus Fibrosus," *Ann. Biomed. Eng.*, **32**, pp. 92–102.
- [26] Demirkoparan, H., and Pence, T. J., 2006, "Swelling of an Internally Pressurized Nonlinearly Elastic Tube With Fiber Reinforcing," *Int. J. Solids Struct.*, in press.
- [27] Demirkoparan, H., and Pence, T. J., 2007, "The Effect of Fiber Recruitment on the Swelling of a Pressurized Anisotropic Nonlinearly Elastic Tube," *Int. J. Non-Linear Mech.*, **42**(2), pp. 258–270.
- [28] Wagner, D. R., and Lotz, J. C., 2004, "Theoretical Model and Experimental Results for the Nonlinear Elastic Behavior of Human Annulus Fibrosus," *J. Orthop. Res.*, **22**, pp. 901–909.
- [29] Billiar, K. L., and Sacks, M. S., 2000, "Biaxial Mechanical Properties of the Natural and Glutaraldehyde Treated Aortic Valve Cusp. Part II: A Structural Constitutive Model," *ASME J. Biomech. Eng.*, **122**, pp. 327–335.
- [30] Sacks, M. S., 2003, "Incorporation of Experimentally Derived Fiber Orientation Into a Structural Constitutive Model for Planar Collagenous Tissues," *J. Biomed. Eng.*, **125**, pp. 280–287.
- [31] Caner, F. C., and Carol, I., 2006, "Microplane Constitutive Model and Computational Framework for Blood Vessel Tissue," *ASME J. Biomech. Eng.*, **128**(3), pp. 419–427.
- [32] Driessen, N. J. B., Bouten, C. V. C., and Baaijens, F. P. T., 2005, "A Structural Constitutive Model for Collagenous Cardiovascular Tissue Incorporating the Angular Fiber Distribution," *ASME J. Biomech. Eng.*, **127**, pp. 494–503.
- [33] Gasser, C. T., Ogden, R. W., and Holzapfel, G., 2006, "Hyperelastic Modelling of Arterial Layers With Distributed Collagen Fiber Orientations," *J. R. Soc., Interface*, **3**(6), pp. 15–35.
- [34] Peng, X. Q., Guo, Z. Y., and Moran, B., 2006, "An Anisotropic Hyperelastic Constitutive Model With Fiber-Matrix Interaction for the Human Annulus Fibrosus," *ASME J. Appl. Mech.*, **73**(5), pp. 815–824.
- [35] Guo, Z. Y., Peng, X. Q., and Moran, B., 2006, "A Composites-Based Hyperelastic Constitutive Model for Soft Tissue With Application to the Human Annulus Fibrosus," *J. Mech. Phys. Solids*, **54**(9), pp. 1952–1971.
- [36] Guo, Z. Y., Peng, X. Q., and Moran, B., 2007, "Mechanical Response of Neo-Hookean Fiber Reinforced Incompressible Nonlinearly Elastic Solids," *Int. J. Solids Struct.*, **44**(6), pp. 1949–1969.
- [37] Guo, Z. Y., Peng, X. Q., and Moran, B., 2007, "Large Deformation Response of a Hyperelastic Fibre Reinforced Composite: Theoretical Model and Numerical Validation," *Composites, Part A*, **38**, pp. 1842–1851.
- [38] Carol, I., Jirásek, M., and Bažant, Z. P., 2004, "A Framework for Microplane Models at Large Strain, With Application to Hyperelasticity," *Int. J. Solids Struct.*, **41**(2), pp. 511–557.
- [39] Malvern, L. E., 1969, *Introduction to the Mechanics of Continuous Medium*, Prentice-Hall, Englewood Cliffs, NJ.
- [40] Ogden, R. W., 1984, *Non-Linear Elastic Deformations*, Wiley, New York.
- [41] Bažant, Z. P., Caner, F. C., Carol, I., Adley, M. D., and Akers, S. A., 2000, "Microplane Model M4 for Concrete. I: Formulation With Work-Conjugate Deviatoric Stress," *J. Eng. Mech.*, **126**(9), pp. 944–953.
- [42] Caner, F. C., and Bažant, Z. P., 2000, "Microplane Model M4 for Concrete. II: Algorithm and Calibration," *J. Eng. Mech.*, **126**(9), pp. 954–961.
- [43] Bažant, Z. P., and Zi, G.-S., 2003, "Microplane Constitutive Model for Porous Isotropic Rocks," *J. Geophys. Res., [Solid Earth]*, **108**(B2), pp. 2119–2129.
- [44] Brocca, M., and Bažant, Z. P., 2000, "Microplane Constitutive Model and Metal Plasticity," *Appl. Mech. Rev.*, **53**(10), pp. 265–281.
- [45] Brocca, M., Brinson, L. C., and Bažant, Z. P., 2002, "Three-Dimensional Constitutive Model for Shape Memory Alloys Based on Microplane Model," *J. Pharm. Sci.*, **50**(5), pp. 1051–1077.
- [46] Caner, F. C., Bažant, Z. P., and Cervenka, J., 2002, "Vertex Effect in Strain-Softening Concrete at Rotating Principal Axes," *J. Eng. Mech.*, **128**(1), pp. 24–33.
- [47] Holzapfel, G. A., 2003, "Structural and Numerical Models for the (Visco)Elastic Response of Arterial Walls and Residual Stresses," *Biomechanics of Soft Tissue in Cardiovascular Systems*, G. A. Holzapfel and R. W. Ogden, eds., Springer, New York, pp. 109–184.
- [48] Belytschko, T., Liu, W., and Moran, B., 2004, *Nonlinear Finite Elements for Continua and Structures*, Wiley, New York.
- [49] Ogden, R. W., 1976, "Volume Changes Associated With the Deformation of Rubber-Like Solids," *J. Mech. Phys. Solids*, **24**, pp. 323–338.
- [50] Cescotto, S., and Fonder, G., 1979, "A Finite Element Approach for Large Strains of Nearly Incompressible Rubber-Like Materials," *Int. J. Solids Struct.*, **15**, pp. 589–605.
- [51] Sussman, T., and Bathe, K., 1987, "A Finite Element Formulation for Nonlinear Incompressible Elastic and Inelastic Analysis," *Comput. Struct.*, **26**, pp. 357–409.

- [52] Oakley, D. R., and Knight, N. F., 1995, "Adaptive Dynamic Relaxation Algorithm for Non-Linear Hyperelastic Structures Part I: Formulation," *Comput. Methods Appl. Mech. Eng.*, **126**, pp. 67–89.
- [53] Bažant, Z. P., 2005, private communication.
- [54] Stroud, A. H., 1971, *Approximate Calculation of Multiple Integrals*, Prentice-Hall, Englewood Cliffs, NJ.
- [55] Bažant, Z. P., and Oh, B.-H., 1986, "Efficient Numerical Integration on the Surface of a Sphere," *ZAMM*, **66**(1), pp. 37–49.
- [56] Boerboom, R., Driessen, N., Bouten, C. V. C., Huyghe, J. M., and Baaijens, F. P. T., 2003, "Finite Element Model of Mechanically Induced Collagen Fiber Synthesis and Degradation in the Aortic Valve," *Ann. Biomed. Eng.*, **31**(9), pp. 1040–1053.
- [57] Wagenseil, J. E., Elson, E. L., and Okamoto, R. J., 2004, "Cell Orientation Influences the Biaxial Mechanical Properties of Fibroblast Populated Collagen Vessels," *Ann. Biomed. Eng.*, **32**(5), pp. 720–731.
- [58] Wang, J. H. C., Jia, F., Gilbert, T. W., and Woo, S. L., 2003, "Cell Orientation Determines the Alignment of Cell-Produced Collagenous Matrix," *ASME J. Biomech. Eng.*, **36**(1), pp. 97–102.